NJC

ROYAL SOCIETY OF CHEMISTRY

PAPER

View Article Online
View Journal | View Issue

Cite this: *New J. Chem.*, 2021, **45**, 2614

A novel fluorescent probe with high photostability for imaging distribution of RNA in living cells and tissues†

Zhaomin Wang,[a] Yong Liu,[a] Weishan Wang,[a] Chang Zhao[a] and Weiying Lin *[ab]

Received 28th October 2020,
Accepted 17th December 2020

DOI: 10.1039/d0nj05286h

rsc.li/njc

RNA has always been valued by scientists in the field of biomedicine, especially biochemistry. Exploring the action and distribution of RNA in the biological environment can help us to gain a deeper understanding of organisms. Although several RNA probes have been developed over the years, it is still necessary to develop more robust RNA probes. Herein, we firstly applied bithiophene to design the novel RNA probe **BT-PHIT** by modifying 2,2′-bithiophene. The new probe can specifically recognize endogenous RNA in cells and tissues to produce a clear fluorescent image. Interestingly, **BT-PHIT** has better photostability and longer tissues imaging depths than traditional RNA probes. Additionally, the robust probe has a large stokes shift and fine membrane permeability.

Introduction

Fluorescent probes are powerful tools and play an important role in many fields such as biological research, diagnosis and treatment of diseases.[1,2] Due to the simplicity and sensitivity of fluorescent probes, various fluorescence imaging techniques have been developed rapidly in recent years.[3–8] Many traditional dyes have been incorporated into fluorescent probes for fluorescence imaging to be used in various fields.[9,10] Fluorescent probes can image otherwise invisible structures in biological environments and realize non-invasive visualization.[11,12] In a sense, the development of fluorescent probes has promoted our understanding of biological science.[13]

Ribonucleic acid (RNA) is an extremely important carrier of genetic material. It is distributed mainly in the nucleolus and cytoplasm of biological cells. RNA has an important role in many aspects of cell life activities.[14] Since the discovery of RNA, protein coding has been considered as its main function.[15–17] RNA is widely involved in gene regulation.[18–20] RNA is not only a bridge between DNA and protein, involved in gene expression and signal transmission, but also a catalyst in many specific reactions.[21,22] Since RNA was discovered, scientists have been exploring its nature, functions and distribution. However, exploration of RNA requires better tools, and so it is necessary to develop better RNA probes.

In recent years, some studies on RNA probes have been reported. For instance, Elhussin *et al.*[23] synthesized an RNA probe based on quinine, which can target RNA in the second near-infrared window with fluorescence enhancement. Yoshino *et al.*[24] successfully synthesized another low biological toxicity RNA probe based on quinoline and applied the probe to image endogenous RNA in the nucleoli of a living cell. In addition, some RNA probes based on benzothiazole, indole and carbazole have been synthesized.[25] They each have different characteristics and functions. However, few RNA probes have outstanding performance in photostability. Even commercialized RNA dyestuffs with unpublished structures are not very good at photostability.

Most of the RNA probes that are developed at present are based on quinoline, indole and benzothiazole.[23–27] The structures of these hosts are likely to be the main reason affecting photobleaching tolerance. Therefore, we tried to use a novel bithiophene structure as the matrix in the hope of developing an RNA probe with high photostability. Bithiophene is a compound similar to carbazole and has a wide range of optical and electrochemical properties.[28,29] In the field of RNA probes, bithiophene has not been used as a substrate.

As we all know, RNA is a single stranded structure made up of many bases, and these bases caused a groove structure. When a probe intercalates with these grooves, the wavelength or intensity of the emission fluorescence of the probe may change.[30,31] Therefore, RNA probes were usually designed in light of this intercalation effect. It has been reported that small molecular compounds with a V-conjugated structure can detect RNA using the embedding mechanism.[32]

[a] *Institute of Fluorescent Probes for Biological Imaging, School of Materials Science and Engineering, School of Chemistry and Chemical Engineering, University of Jinan, Jinan, Shandong 250022, P. R. China. E-mail: weiyinglin2013@163.com*
[b] *Guangxi Key Laboratory of Electrochemical Energy Materials, Institute of Optical Materials and Chemical Biology, School of Chemistry and Chemical Engineering, Guangxi University, Nanning, Guangxi 530004, P. R. China*

† Electronic supplementary information (ESI) available: Experimental details including synthesis, characterization of the compounds, absorption and fluorescence spectroscopic data, and living cell imaging. See DOI: 10.1039/d0nj05286h

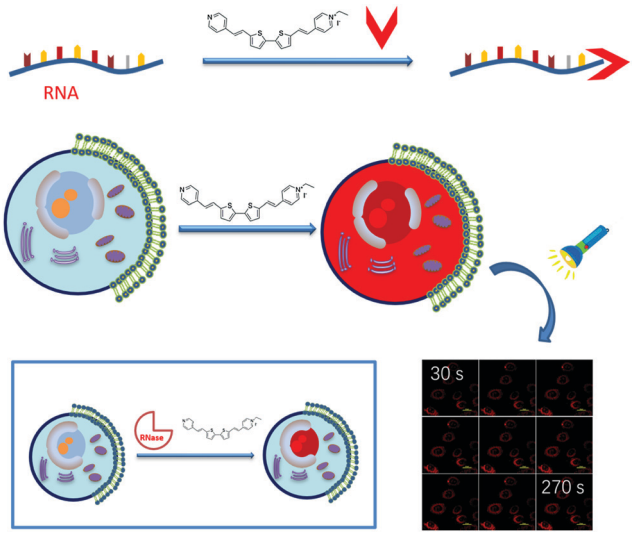

Fig. 1 Sensing strategies of the probe **BT-PHIT** to RNA.

Based on this information, we synthesized an RNA probe **BT-PHIT** with a novel structure by modifying bithiophene. We connected pyridine with 2,2′-bithiophene by a coupling reaction and modified one end with iodoethane to form a V-conjugated structure. **BT-PHIT** has fluorescence emission in the range of 570–620 nm in the nucleolus and cytoplasm under the excitation wavelength of 488 nm. First, we demonstrated that the fluorescence emission of the probe was caused by endogenous RNA in cells by enzymatic verification. Then, we investigated the photostability of **BT-PHIT** by comparing commercial probes. Finally, we tested the imaging depth of the probe using mouse liver tissue. Interestingly, **BT-PHIT** has a higher photostability than conventional probes and a deeper imaging depth than commercial probes (Fig. 1).

Experimental

General procedure and spectral measurements

Preparation of samples: the probe **BT-PHIT** was made into a 1 mM solution with DMF. In the photophysical experiments, the mother liquor was diluted to 5 μM with the solvent.

Preparation of test samples for detection: in the experiment investigating the response of the probe **BT-PHIT** to RNA, the test samples for detection were obtained by dissolving $BaCl_2$, $CuSO_4$, $FeCl_3$, K_2CO_3, $MgCl_2$, $NaNO_3$, and NH_4Ac in deionized water. RNA and DNA test solution were obtained by dissolving RNA or DNA in Tris-buffer solution. By rough calculation, an appropriate amount of RNA or DNA was weighed and dissolved in Tris-buffer solution. The specific concentration was calculated using the Lambert–Beer formula and UV spectrum measurement (for details, see the calculation method of RNA and DNA concentration in the ESI†).

Parameters for spectral measurements: the excitation wavelength was 460 nm, the excitation slit width was 5 nm and the emission slit width was 5 nm.

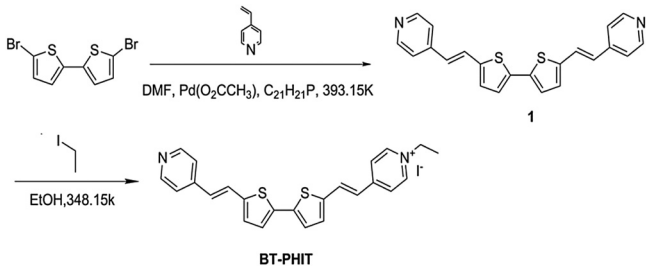

Scheme 1 The synthetic route of the probe **BT-PHIT**.

Cell culture and imaging

Composition of cell culture medium: the volume ratio of DMEM (Dulbecco's Modified Eagle's Medium), fetal bovine serum and penicillin was 100 : 10 : 1. Cells were cultured in the CO_2 constant temperature incubator. Cells were transferred to confocal dishes 24 hours before imaging using a Nikon AMP1 laser scanning confocal microscope. The cell coverage rate reached about 70% before imaging of the cell. In the experimental and control groups, the culture medium containing probe **BT-PHIT** (10 μM) was used for 30 minutes before imaging, and then PBS solution was used for cleaning. After cleaning, PBS was removed and new culture medium was added for imaging.

RNase digestion test

After live cell imaging, an RNase digestion test was carried out, according to the previous reports. First, two groups of cells with 70% cell coverage were cultured in confocal plates. The cells in both groups were fixed with 1 mL 4% formalin-fixed solution for 3 h. Then cells of both groups were pierced using 5% Triton X-100 for 120 s and washed with PBS. Then, 1 mL PBS with 4 μL RNase (5 mg mL^{-1}) was added to one group for 2 h. The control group had a clean 1.004 mL of PBS added for the same time of 2 h. Finally, the two groups of cells were stained with **BT-PHIT** and imaged.

Tissue imaging

The biological tests were approved by the Institutional Animal Care and Use Committee of Shandong University. All animal procedures were performed in accordance with the Guidelines for Care and Use of Laboratory Animals of Shandong University and approved by the Animal Ethics Committee of Shandong University. Liver tissue was taken from 7-week-old mice. Five-week-old mice were bought from the School of Pharmaceutical Sciences, Shandong University. They were fed for two weeks, and liver tissue sections were taken for tissue imaging.

Synthetic procedures

Synthesis routine of 1. Compound 5,5′-dibromo-2,2′-bithiophene (0.321 g, 1.0 mmol) was dissolved in DMF (30 mL). K_2CO_3 (0.414 g, 3.0 mmol), palladium(II) acetate (0.022 g, 0.1 mmol) and tri(*o*-tolyl)phosphine (0.068 g, 0.2 mmol) were added. Then mixture was protected by N_2 and heated to 313.15 K. 4-Vinyl pyridine (0.315 g, 3.0 mmol) was

Table 1 The photophysical properties of **BT-PHIT** in various solvents

Solvents	λ^a (nm)	λ^b (nm)	Φ^c
PBS	455	622	0.058
H_2O	460	624	0.068
DMF	455	631	0.090
MeOH	462	627	0.081
MeCN	456	630	0.081

[a] Maximum absorption wavelength (nm). [b] Maximum fluorescence emission wavelength (nm). [c] Φ is the fluorescence quantum yield (error limit: 8%) determined by using rhodamine 6G (F = 0.95) in water as the standard.

added using a syringe. The solution mixture was allowed to reflux for 72 h at 393.15 K (Scheme 1).

Synthesis routine of BT-PHIT. 1 (0.534 g, 1.0 mmol) and iodoethane (0.234 g, 1.5 mmol) were dissolved in absolute ethyl alcohol (100 mL). The solution mixture was allowed to reflux for 72 h at 353.15 K. ^{1}H NMR (400 MHz, DMSO, δ): 8.953 (d, J = 5.8 Hz, 2H; pyridine), 8.554 (d, J = 5.8 Hz, 2H; pyridine), 8.239 (d, J = 16.4 Hz, 1H; CH═CH), 8.210 (d, J = 6.8 Hz, 2H; pyridine), 7.765 (d, J = 16.0 Hz, 1H; CH═CH), 7.552 (d, J = 6.0 Hz, 2H; pyridine), 7.525 (d, J = 4.0 Hz, 1H; thiophene), 7.502 (d, J = 5.2 Hz, 1H; thiophene), 7.483 (d, J = 3.6 Hz, 1H; thiophene), 7.360 (d, J = 4.0 Hz, 1H; thiophene), 7.184 (d, J = 16.0 Hz, 1H; CH═CH), 7.6.982 (d, J = 16.0 Hz, 1H; CH═CH), 4.531 (q, J = 7.2 Hz, 2H; CH_2), 1.526 (t, J = 7.2 Hz, 3H; CH_3). ^{13}C NMR, (400 MHz, DMSO-d) δ (ppm): HRMS (m/z): 150.760, 150.525, 144.330, 144.134, 142.302, 140.188, 140.037, 136.406, 133.915, 133.823, 130.666, 126.882, 126.500, 126.393, 123.941, 123.941, 122.625, 121.188, 55.642, 21.562, 16.638. $[M - I]^+$ calcd for $C_{24}H_{21}N_2S_2^+$: 401.1141; found: 401.1141.

Results and discussion

Spectral measurements of BT-PHIT

Firstly, we measured the absorption spectrum and emission spectrum of compound **BT-PHIT**. In several different solutions, the absorption wavelength of the compound is concentrated in the range of 455–460 nm. The strongest emission peak of the probe **BT-PHIT** in DMF appears at 631 nm, and the strongest emission peak in the water system appears at about 624 nm. It is important that the compound exhibits a large Stokes shift (about 160 nm) in both aqueous and organic solvent systems. Stokes shift is a very important scale to measure the superiority

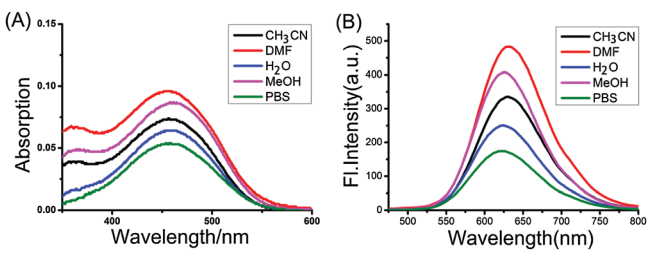

Fig. 2 (A) Absorption spectra and (B) fluorescence responses of **BT-PHIT** in various solvents; [**BT-PHIT**]: 5 μM.

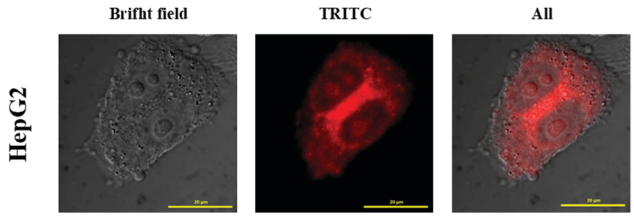

Fig. 3 Confocal fluorescence images of living HepG2 cells incubated with **BT-PHIT**. Red fluorescence images were collected under excitation at 488 nm. Scale bar: 20 μm.

of the probe. As is known to all, when the probe is used for detection, the larger the Stokes shift, the smaller the error. In addition, the fluorescence quantum yield of the probe is about 8% in each system, and the corresponding quantum yield in the organic system is relatively higher (Table 1 and Fig. 2, quantum yields in the ESI†).

Then, in order to explore whether the probe can recognize RNA *in vitro*, we carried out RNA titration *in vitro*. The probe was dissolved in Tris–HCl buffer solution and maintained at a specific concentration (1 μm), and the concentration of RNA in the solution was increased during the measurement of fluorescence spectrum. A graph of the change of probe fluorescence intensity with RNA concentration was obtained (Fig. S1 in the ESI†). Up to 700 equivalents of RNA, the fluorescence intensity of the probe at 620 nm positively correlated with the change in

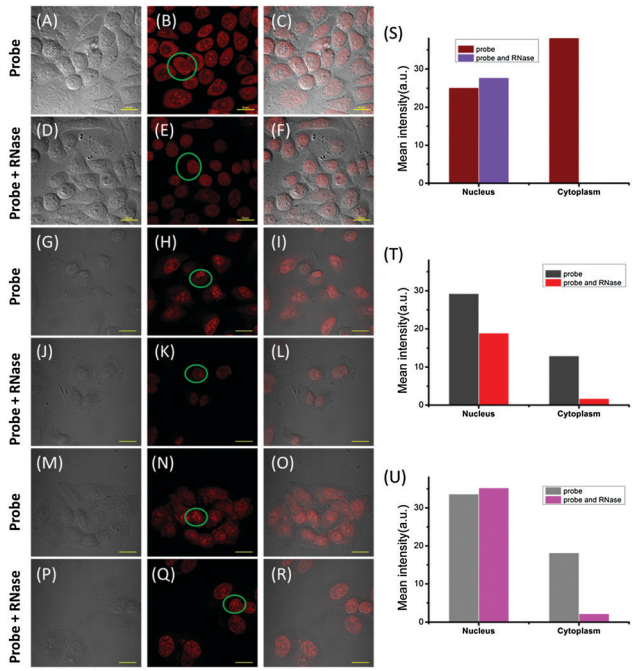

Fig. 4 RNase digest experiment. All fluorescence imaging pictures of fixed cells stained with **BT-PHIT** (10 μM). Imaging picture of HeLa (A–C), A549 (G–I), and HepG2 (M–O) cells not treated with RNase. Imaging pictures of HeLa (D–F), A549 (J–L), and HepG2 (P–R) treated with RNase. (S–U) Mean fluorescence intensity of the cytoplasm and nucleus before and after treatment with RNase. λ_{ex} = 488 nm, λ_{em} = 570–620 nm, and bar = 20 μm.

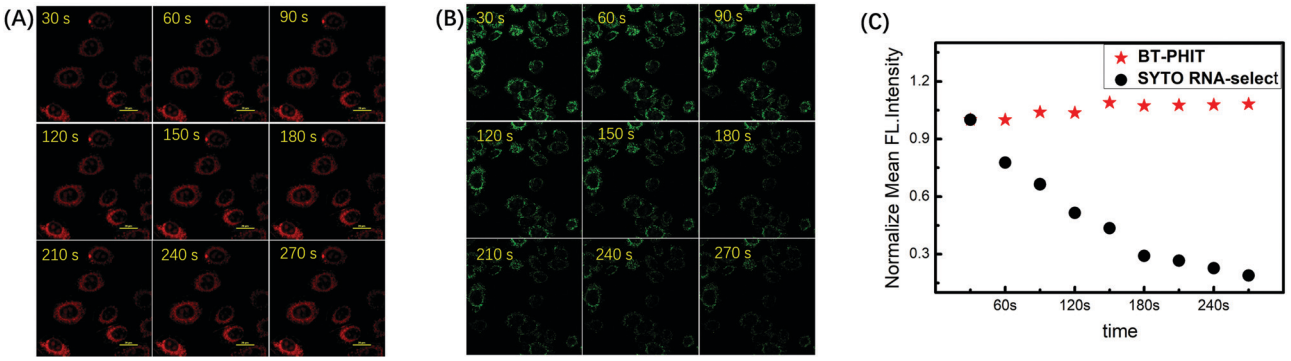

Fig. 5 Comparison of photobleaching of **BT-PHIT** and SYTO RNA-Select in confocal fluorescence microscopy imaging. (A) Image of living HeLa cells incubated with **BT-PHIT**. (B) Image of living HeLa cells incubated with SYTO RNA-Select. (C) Change of normalized mean fluorescence intensity of **BT-PHIT** and SYTO RNA-Select with time. [**BT-PHIT**]: 10 μM, [SYTP RNA-select]: 10 μM, λ_{ex} = 488 nm, bar = 20 μm.

RNA concentration. When the RNA concentration increased 700-fold, the fluorescence intensity stabilized at about two times the original intensity. According to the experimental results, a change in fluorescence intensity at 630 nm was selected to draw a scatter plot so as to study the detection limit of the probe using the regression equation. The results show that the probe has an above average sensitivity (Fig. S2 in the ESI†).

Furthermore, various analytes including anions, cations, reducing agents, active oxides and common amino acids were used to test the probe **BT-PHIT** in Tris–HCl buffer solution and the results were compared with those of RNA to further test the ion selectivity of **BT-PHIT** (Fig. S3 in the ESI†). The analytes of the cations including Ca^{2+}, Cu^{2+}, Fe^{3+}, K^{+}, Mg^{2+}, Na^{+}, Ni^{+}, and Zn^{+}, anions including Br^{-}, Cl^{-}, I^{-}, NO_3^{-}, and SO_4^{2-}, reducing agents SO_3^{2-}, active oxides NO_2^{-} and amino acids L-cysteine (Cys) elicited no marked response. However, RNA with the same concentration as other ions except Cys could double the fluorescence intensity of the probe at the same excitation wavelength. The influence of DNA is almost inevitable for RNA probes that are based on an embedding mechanism. Therefore, we focus on the influence of DNA on detection. By testing, RNA and DNA caused a red-shift of probe absorption in buffer solution. However, the same concentration of RNA made the probe have a longer red-shift than DNA (Fig. S4 in the ESI†). We carried out titration experiments with RNA and DNA, respectively, at λ_{ex} = 488 nm. The results showed that the fluorescence intensity of the probe in buffer solution with RNA was higher than that with the same concentration of DNA (Fig. S5 in the ESI†). In order to test the stability of the probe in buffer solution, three groups of stability tests were carried out. The results showed that the probe has high stability whether it exists alone or with DNA and RNA (Fig. S6 in the ESI†).

Imaging of endogenous RNA in living cells

The above experiment proved that probe **BT-PHIT** could specifically check RNA *in vitro*. Moreover, water-soluble small molecules easily enter the cell through the pores on the membrane. We therefore speculated that **BT-PHIT** can mark endogenous RNA of living cells. So, we used the probe for imaging living cells.

First, we measured the biological toxicity of probe **BT-PHIT** to cells using the standard 3-(4,5-dimethyl-2-thiazoly)-2,5-diphenyl-2-*H*-tetrazolium bromide (MTT) assays prior to the imaging. The results of the toxicity test showed that the probe has relatively low toxicity to cells (Fig. S7 in the ESI†). Then, we cultured the cells with **BT-PHIT** and imaged them using a laser confocal microscope. As was expected, at λ_{ex} = 488 nm, a clear fluorescence signal was observed in the red channel. According to the image, the area of fluorescence signal mainly appears in the nucleus and cytoplasm (Fig. 3). Therefore, we speculate that the fluorescence signal may be caused by endogenous RNA of living cells.

The RNase digest experiment

Based on our conjecture, we carried out the digest test using RNase (ribonuclease). We cultured three kinds of cancer cells (HeLa, A549, and HepG2) in a constant temperature incubator. Each kind of cell was divided into two groups. The other conditions were the same after fixing and drilling. The only variable was whether RNase was added. Then experimental groups and control groups were imaged using a confocal laser scanning microscope at 488 nm. Images of six groups of fixing cells were obtained. Then, the mean fluorescence intensity of different positions was counted using ImageJ software, and the histogram was plotted (Fig. 4).

In the test group and blank control group of the three kinds of cells, the probe **BT-PHIT** produced clear fluorescence images in the red channel. In the control group of HeLa cells, the red fluorescence appeared in the cytoplasm and nucleus (Fig. 4A–C). In the RNase digested group, the fluorescence disappeared in the cytoplasm, and strong fluorescence was shown in the nucleus (Fig. 4D–F). As shown in Fig. 4S, the cells without RNase digestion showed fluorescence signals distributing in the nucleus and cytoplasm, and the average fluorescence intensity in the cytoplasm was higher than that in the nucleus. After digestion by RNase, the fluorescence intensity in the cytoplasm was almost zero, and the average fluorescence intensity in the nucleus increased

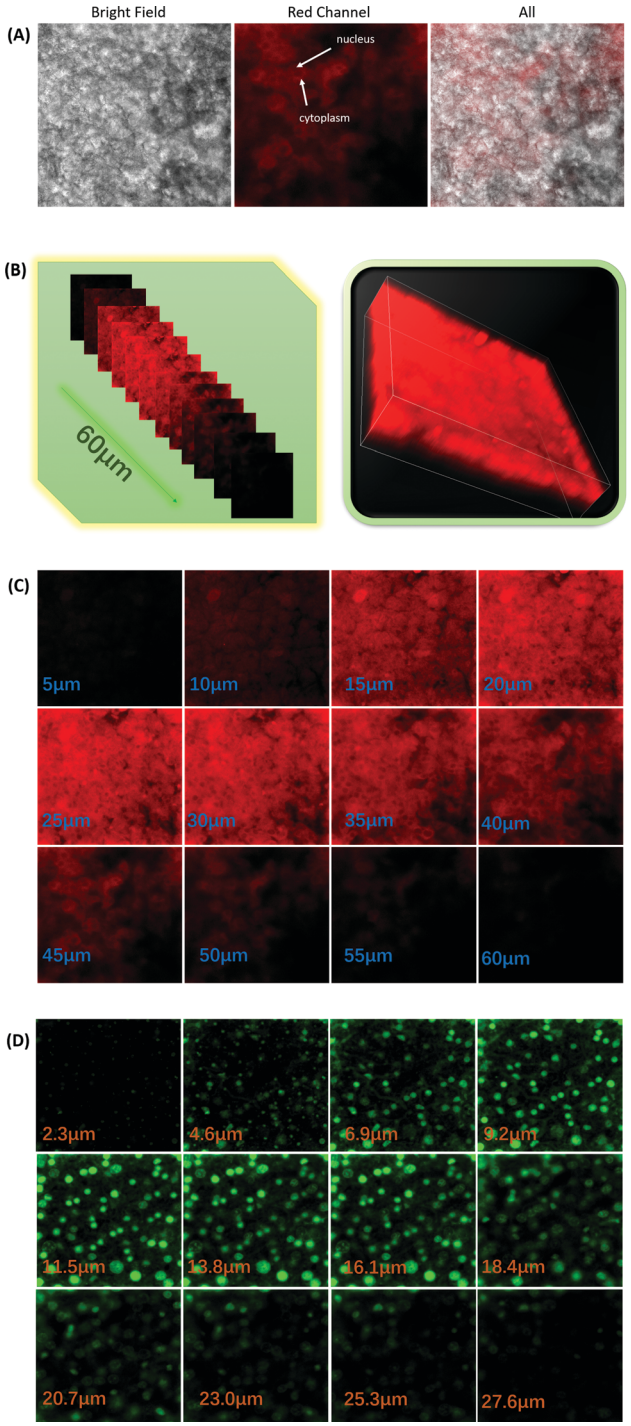

Fig. 6 (A) Confocal fluorescence images of mouse tissue incubated with **BT-PHIT** (10 μM); (B) 3D fluorescence images. Red channel (λ_{ex} = 488 nm, λ_{em} = 570–620 nm); (C) tissue fluorescence imaging of **BT-PHIT** at different depths; (D) tissue fluorescence imaging of SYTO RNA-Select at different depths.

slightly. In the other two groups of cancer cells (HepG2 and A549), the fluorescence signal of the control group and experimental group is also significantly different. The fluorescence signal in the cytoplasm of the experimental group is much lower than that of the control group (Fig. 4M–R). In order to reflect this difference more intuitively, we plotted the average fluorescence intensity of different regions into a column graph (Fig. 4T and U). Experiments of several groups had proved that the fluorescence signal of **BT-PHIT** is caused by endogenous RNA of living cells.

Optical stability of BT-PHIT

Photostability is an important factor to evaluate the quality of the probe.[33,34] Therefore, we conducted experiments to test the photostability of **BT-PHIT**. Culture medium with **BT-PHIT** (10 μM) was used to produce HeLa cells and the cells in the imaging dish were continuously scanned for 5 min using a confocal microscope after being washed with PBS. As shown in Fig. 5A, there was almost no change in the fluorescence image of **BT-PHIT** within 5 minutes. In order to make the experimental results more intuitive, we used commercial probe SYTO RNA-Select replacing the probe **BT-PHIT** to image under the same conditions, and compared the two probes. As shown in Fig. 5B, the fluorescence signal of SYTO RNA-Select was obviously quenched by light in the living cells. In contrast, **BT-PHIT** had better photostability than the commercial probe (Fig. 5C).

Imaging of tissue of mice

In order to further explore the application of the probe **BT-PHIT**, we conducted a tissue imaging experiment using mice liver tissue. The liver tissue of mice was taken out and sliced. Then the tissue sections were incubated in PBS with **BT-PHIT** (10 μM) for 2 h. Then the liver tissue section of mice was put in an imaging dish and imaged using 488 nm excitation wavelength. We found that probe **BT-PHIT** could show a fluorescence signal in the cytoplasm and nucleus of mouse tissue cells (Fig. 6A). And the fluorescence signal of probe **BT-PHIT** in the cytoplasm was found to be slightly stronger than that in the nucleus. This is consistent with the previous results in living cells. So, we infer that the fluorescence signal was caused by endogenous RNA of mouse tissue cells.

Furthermore, the tissue imaging depth of **BT-PHIT** was tested using a tomoscan experiment. We obtained three-dimensional fluorescence images using a 488 nm excitation wavelength microscope, (Fig. 6B). We found that the probe can be used for the fluorescence imaging of mouse liver tissue with about 50 μm depth (Fig. 6C). A commercial probe was used for comparison. Mice tissue was incubated in PBS with SYTO RNA-Select under the same conditions, and the tomoscan experiment was performed. The results show that the imaging depth of SYTO was about 25 μm (Fig. 6D). Therefore, we can conclude that the imaging depth of the probe **BT-PHIT** is excellent.

Conclusion

To sum up, we synthesized a novel RNA probe **BT-PHIT** by decorating bithiophene. **BT-PHIT** has several favorable features, such as larger stokes shift, small biological toxicity, great membrane permeability and long tissue imaging depth. More interestingly, **BT-PHIT** has better photostability than the

conventional probes. In addition, this is the first time that bithiophene has been used in the field of RNA probes, and this may provide a new strategy for the development of RNA probes.

Conflicts of interest

There are no conflicts to declare.

Acknowledgements

This work was financially supported by NSFC (21672083, 51503077, 21877048, 51973082, 22077048), Taishan Scholar Foundation (TS 201511041), the startup fund of the University of Jinan (309-10004), Doctor start up fund of University of Jinan (160082102) and NSFSP (ZR2015PE001).

Notes and references

1 G. M. van Dam, G. Themelis, L. M. A. Crane, N. J. Harlaar, R. G. Pleijhuis, W. Kelder, A. Sarantopoulos, J. S. de Jong, H. J. G. Arts, A. G. J. van der Zee, J. Bart, P. S. Low and V. Ntziachristos, *Nat. Med.*, 2011, **17**, 1315–1319.
2 H. Kobayashi and P. L. Choyke, *Acc. Chem. Res.*, 2010, **44**, 83–90.
3 L. Yuan, W. Lin, L. Tan, K. Zheng and W. Huang, *Angew. Chem., Int. Ed.*, 2013, **52**, 1628–1630.
4 L. He, X. Yang, K. Xu, X. Kong and W. Lin, *Chem. Sci.*, 2017, **8**, 6257–6265.
5 Y. Tang, X. Kong, Z. Liu, A. Xu and W. Lin, *Anal. Chem.*, 2016, **88**, 9359–9363.
6 P. Ning, W. Wang, M. Chen, Y. Feng and X. Meng, *Chin. Chem. Lett.*, 2017, **28**, 1943–1951.
7 W. Xu, Z. Zeng, J. Jiang, Y. Chang and L. Yuan, *Angew. Chem., Int. Ed.*, 2016, **55**, 13658–13699.
8 H. Zhu, J. Fan, J. Du and X. Peng, *Acc. Chem. Res.*, 2016, **49**, 2115–2126.
9 X. H. Gao, Y. Y. Cui, R. M. Levenson, L. W. K. Chung and S. M. Nie, *Nat. Biotechnol.*, 2004, **22**, 969–976.
10 M. J. Rust, M. Bates and X. Zhuang, *Nat. Methods*, 2006, **3**, 793–795.
11 W. Shu, S. Zang, C. Wang, M. Gao, J. Jing and X. Zhang, *Anal. Chem.*, 2020, **92**, 9982–9988.
12 W. Shu, Y. Wu, S. Zang, S. Su, H. Kang, J. Jing and X. Zhang, *Sens. Actuators, B*, 2020, **303**, 127284.
13 M. R. Gill, J. Garcia-Lara, S. J. Foster, C. Smythe, G. Battaglia and J. A. Thomas, *Nat. Chem.*, 2009, **1**, 662–667.
14 R. E. Johnston and H. R. Bose, *Proc. Natl. Acad. Sci. U. S. A.*, 1972, **69**, 1514–1516.
15 Y. Ota, A. Kikuchi and M. Cashel, *Proc. Natl. Acad. Sci. U. S. A.*, 1979, **76**, 5799–5801.
16 L. C. Gerstenfeld, S. D. Chipman, C. M. Kelly, K. J. Hodgens, D. D. Lee and W. J. Landis, *J. Cell Biol.*, 1988, **106**, 979–989.
17 S. Yamashita and S. Melmed, *J. Clin. Invest.*, 1986, **78**, 1008–1014.
18 P. A. Sharp, *Cell*, 2010, **136**, 577–580.
19 F. Michelini, A. P. Jalihal, S. Francia, C. Meers, Z. T. Neeb, F. Rossiello, U. Gioia, J. Aguado, C. J. Weinert, B. Luke, G. Biamonti, M. Nowacki, F. Storici, P. Carninci, N. G. Walter and F. D. D. Fagagna, *Chem. Rev.*, 2018, **118**, 4365–4403.
20 A. Bastide and A. David, *Biomolecules*, 2018, **8**, 100.
21 K. Kruger, P. J. Grabowski, A. J. Zaug, J. Sands, D. E. Gottschling and T. R. Cech, *Cell*, 1982, **31**, 147.
22 S. Brenner, F. Jacob and M. Meselson, *Nature*, 1961, **190**, 576–581.
23 I. E. H. Elhussin, S. Zhang, J. Liu, D. li, Q. Zhang, S. Li, X. Tian, J. Wu and Y. Tian, *Chem. Commun.*, 2020, **56**, 1859–1862.
24 Y. Yoshino, Y. Sato and S. Nishizawa, *Anal. Chem.*, 2019, **91**, 14254–14260.
25 Y. Ma, J. Yin, G. Li, W. Gao and W. Lin, *Coord. Chem. Rev.*, 2020, **406**, 213144.
26 Y. Yoshino, Y. Sato and S. Nishizawa, *Anal. Chem.*, 2019, **91**, 14254–14260.
27 T. Chiba, T. Sato, Y. Sato and S. Nishizawa, *Org. Biomol. Chem.*, 2017, **15**, 7765–7769.
28 B. Czaplinska, A. Maron, J. G. Malecki, G. S. Gorol, M. Matussek, K. Malarz, A. M. Wilczkiewicz, W. Danikiewicz, R. Musiol and A. Slodek, *Dyes Pigm.*, 2017, **114**, 119–132.
29 T. Nakanishi, Y. Shiral and L. Han, *J. Mater. Chem. A*, 2015, **3**, 4229–4238.
30 S. Halder and D. Bhattacharyya, *Prog. Biophys. Mol. Biol.*, 2013, **113**, 264.
31 Q. Yao, H. Li, L. Xian, F. Xu, J. Xia, J. Fan, J. Du, J. Wang and X. Peng, *Biomaterials*, 2018, **177**, 78.
32 G. Song, F. Miao, Y. Sun, X. Yu, J. Z. Sun and W. Y. Wong, *Sens. Actuators, B*, 2012, **173**, 329.
33 H. K. Kleinman, D. Philp and M. P. Hoffman, *Curr. Opin. Biotechnol.*, 2003, **14**, 526–532.
34 F. Pampaloni, E. G. Reynaud and E. H. K. Stelzer, *Nat. Rev. Mol. Cell Biol.*, 2007, **8**, 839–845.